Thermal management of a Formula E electric motor: analysis and optimization*

Marco Cavazzuti[1]†, Gloria Gaspari[1], Stefano Pasquale[2], Enrico Stalio[1]

[1]Dipartimento di Ingegneria "Enzo Ferrari", Università degli Studi di Modena e Reggio Emilia, via P. Vivarelli 10, 41125, Modena, Italy

[2]Magneti Marelli SpA, via A. Borletti 61/63, 20011, Corbetta (MI), Italy

Abstract

The thermal analysis of a high performance brushless synchronous electric motor with permanent magnets and water jacket cooling is presented. The analysis is carried out following a lumped parameter thermal network approach which allows to identify the most important thermal paths in the motor and the main parameters influencing them. Thanks to its simplicity, the solution of such a thermal network model is very fast, allowing a large number of what-if scenarios to be computed over a short amount of time. For this reason, the model is coupled with external tools for performing systematic sensitivity analyses and optimizations. Goal of the investigation is the reduction of the windings temperature being this temperature inversely proportional to the efficiency and the power delivered by the motor. The sensitivity analysis, performed over a series of material, geometric, and operational factors, leads to the identification of the most relevant parameters influencing the thermal behaviour of the motor. A series of optimizations, focusing on these parameters and including suitable constraints granting the well-posedness of the problem and the feasibility of the solution, bring to the definition of an optimum layout of the water jacket and of the stator geometries. The optimized geometry allows a significant reduction of the windings temperature to be achieved.

Keywords

Electric motor, Formula E, Thermal management, Lumped parameter analysis, Optimization

Highlights

- The aim of this work is the thermal optimization of a Formula E electric motor.
- A lumped parameter thermal network model is employed.
- The paths of heat flux in the motor are investigated in detail.

*Preprint version — Paper published on Applied Thermal Engineering, 157:113733, 2019, https://doi.org/10.1016/j.applthermaleng.2019.113733

†Corresponding author: Marco Cavazzuti, email: marco.cavazzuti@unimore.it, tel.: +39 059 2056347

Nomenclature

A	heat transfer surface area	W	width	cnv	convective
g	gradient			in	inlet section
h	heat transfer coefficient	*Greek Symbols*		ln	slot liner
H	height	α	electric resistivity	nm	nominal configuration
L	thickness, depth, or length		temperature coefficient	rad	radiative
$\dot{m}$	mass flow rate	Δ	difference	ref	reference value
M	mass	λ	thermal conductivity	rs	impregnating resing
p	pressure			sl	stator slot
P	power source	*Superscripts*		st	stator lamination
$\dot{Q}$	heat flow	$*$	normalized	th	stator tooth
R	thermal resistance			tot	total
t	time	*Subscripts*		wdg	windings
T	temperature	act	active section	wj	water jacket
V	volume	cnd	conductive	yk	stator yoke

- A sensitivity analysis on the parameters influencing the main heat path is performed.
- The optimization procedure leads to reduced operating temperatures.

1 Introduction

In recent years electric motors have attracted the attention of researchers and automotive companies due to the pressing environmental issues. In particular, they have taken hold in the field of competitions with the inauguration of the ABB FIA Formula E championship in 2014. Formula E is the maximum competition using only electric-powered cars, and represents a privileged environment where advanced solutions that could possibly be adopted in road vehicles are tested. Continuous research is leading to improved car performances and durability. In view of this, the thermal management of the motor, and of the vehicle in general, becomes particularly important, also considering the electric power densities at stake. High temperatures, in fact, are detrimental to the performance and life of several components, and efficient cooling systems are therefore essential. Overheating reduces battery life, degrades the rare earths of the motor magnets, and promotes the dissipation by Joule heating of the copper windings.

Thus, an accurate thermal modelling of the motor and of the coupled cooling system becomes important for the optimal thermal management of the engine. This topic has been dealt with in the literature in different ways. In a thermal model it is necessary first of all to evaluate the heat sources, and then model the conductive, convective and radiative heat transfer paths across the whole motor down to the heat sinks represented by the cooling system. The thermal energy sources derive mainly from the electromagnetic losses (hysteresis and eddy currents in the magnets and in the laminations, and Joule heating in the windings) and can be predicted using electromagnetic Finite Element Analysis

(FEA) simulation software, such as in [1]. Heat transfer and fluid flow can be modelled by means of Computational Fluid Dynamics (CFD) for given sources and boundary conditions, while FEA is only able to simulate conductive heat transfer [2].

Even though detailed 3D simulations of the full motor would be very informative, the computational cost prevents them from being widely applied at the design stage. A few attempts using CFD have been made in the literature, but they are limited to small portions of the motor such as in [3] where the conjugate heat transfer across a finned housing is investigated for given heat flux and ventilation conditions, and in [4] where a new water cooling system made of cold plates in the magnetic core is simulated. Other works present the CFD analysis of different electric motor cooling systems like rotor blades induced ventilation [5], oil spray injection [6], or hollow shaft oil circulation [7].

More often, the thermal analysis of an electric motor has been carried out adopting a Lumped Parameter Thermal Network (LPTN) [8]. With LPTN an equivalent thermal network of the motor consisting of nodes and thermal resistances is created. Each node represents a component or a portion of the machine, and nodes are interconnected by a suitable network of thermal resistances. Thermal energy sources, sinks, or fixed temperatures can be applied as boundary conditions to the nodes, while the resistances are either of the conductive, convective, radiative, or contact type. The network models the thermal behaviour of the motor both radially and axially. The solution of a LPTN is very fast and no more than a few seconds of CPU time are needed for iteratively solving the system of equations of a detailed network on an ordinary PC. In [9] it is shown that a network with as little as ten nodes can already give reasonably good predictions of the operating temperature distribution in the main motor components. Anyhow, the thermal resistances of the LPTN need some calibration, and the quality of the network predictions is strictly correlated to the quality of the calibration. This is particularly true for the many convective resistances that depend on the evaluation of a convective heat transfer coefficient from proper correlations. Similarly for the conductive resistances related to the resin impregnated copper windings: as it is not possible to model every single wire, the set of wires and resin must be treated as a unique non-isotropic but orthotropic material whose axial and radial thermal conductivities need some modelling. The extensive work of Cavagnino *et al.* [10, 11, 12] progressively focused on different aspects of this calibration process in order to improve the predictive capability of the LPTNs. The equivalent thermal conductivity of the impregnated windings is investigated in [13] where a correlation based on the filling factor and the thermal conductivities of the single materials is given for a two materials mixture, and in [14] where a porous metal model is introduced for the same purpose.

In [15] a LPTN is used for predicting the transient behaviour of an electric motor with a phase change cooling system for the end-windings. LPTNs have also been used for modelling a 60 kW permanent magnet synchronous automotive motor in [16], and in [17] for simulating loop heat pipes for the thermal energy management of electric vehicles.

In the present work, the electric motor developed by Magneti Marelli for the 3rd season of the Formula E championship is investigated by means of a LPTN approach. The motor is a Brushless synchronous AC machine with Permanent Magnets (BPM) and a water jacket cooling system. The goal is to reduce the operating temperatures of the motor hot spots, and in particular of the copper

windings, by identifying and optimizing the most influential parameters. A detailed analysis of the motor in its nominal configuration allows to identify the preferential heat flux directions. At first, a sensitivity analysis is carried out on a number of parameters affecting the thermal resistances along these paths. In the second phase, the most influential parameters are included in an optimization process. The sensitivity analysis results suggest possible directions for future research on electric motors, while through the optimization an optimum motor configuration for a given set of constraints is proposed. The LPTN analyses are performed with the commercial software Motor-CAD, while optimization is set up using the freeware software Dakota. The two codes are interfaced by means of Matlab scripts exploiting the ActiveX functions available in Motor-CAD. Matlab scripts control both the sensitivity analysis and the link between the simulation and the optimization software.

2 Lumped parameter thermal model

Sensitivity analyses and optimizations have to rely on a fast solution procedure. In the present research a lumped parameter model is used for this purpose as implemented in Motor-CAD. The software consists of three modules: one for the 2D electromagnetic and electrical performance FEA, one for solving the thermal network from given thermal sources, and the last for computing efficiency maps based on the results coming from the previous two modules. The coupling between the electromagnetic and the thermal modules is one-way: the electromagnetic losses are computed in the former, and the corresponding thermal sources are imposed in the latter. Here we concentrate on the steady-state thermal aspects and use the thermal module only. This means that the electromagnetic losses, coming from previous experimental and numerical analyses, are imposed *a priori*, and the operating conditions of the motor are fixed. The closed-loop analysis carried out in the thermal module for solving the LPTN allows to perform what-if calculations very fast. In this way, the thermal effect of any change to the machine design can be quickly evaluated. This makes the thermal module particularly suitable for the systematic analysis of different motor configurations using external sensitivity analysis and optimization tools.

Once the motor type (a BPM in the current investigation) and the cooling system (*e.g.* water jacket) are defined, the topology of the equivalent thermal network solved by Motor-CAD is determined. The LPTN consists of thermal resistances and nodes, with thermal power sources and temperatures imposed as boundary conditions at specific nodes. The value of the thermal resistances derives from the input data (*e.g.*, geometry, material properties, and cooling system specifications), while by solving the network the temperature at the nodes and the thermal power across each resistance is computed. An example network is shown in Fig. 1. A color is assigned to each motor component like rotor, magnets, stator, copper windings, water jacket. The network represents the geometric structure of the motor both radially and axially. This is graphically represented respectively by vertical and horizontal connections in the scheme of Fig. 1. The network solved is rather complicated and composed by over 100 nodes.

Conductive resistance is defined as

$$R_{\mathrm{cnd}} = \frac{L}{\lambda A}\,, \tag{1}$$

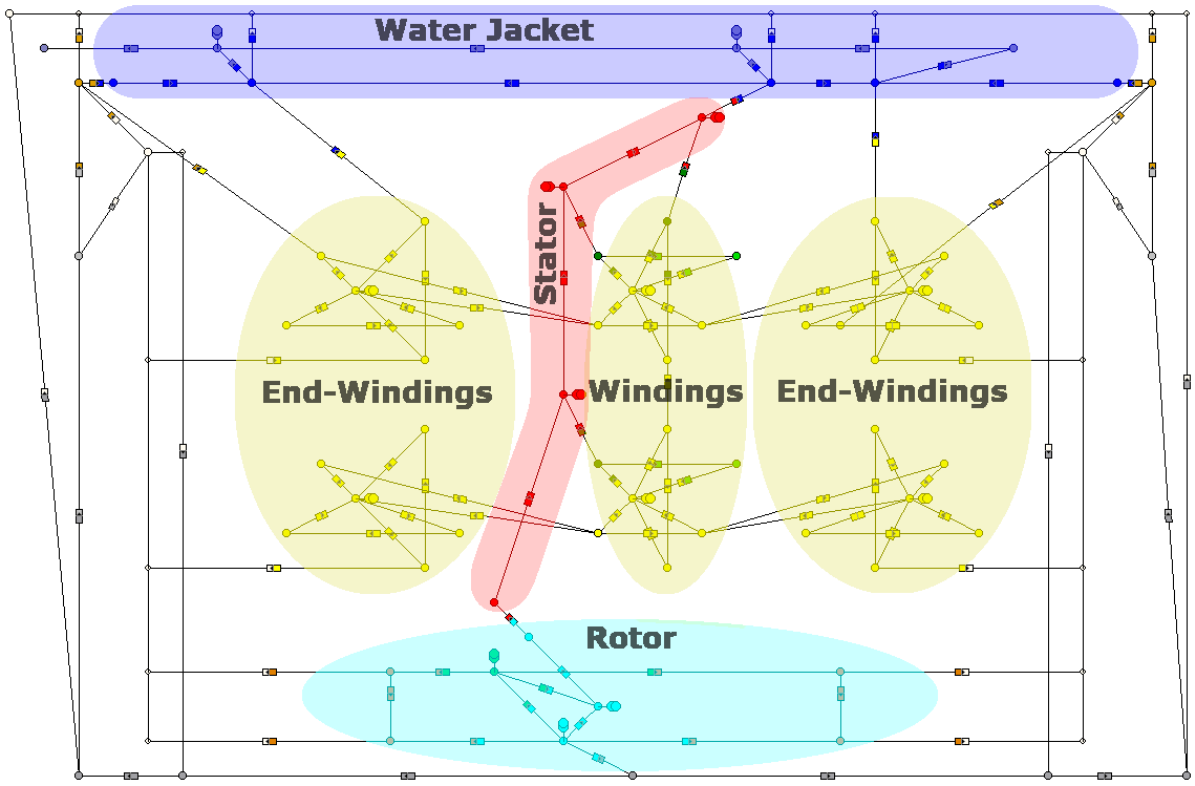

Figure 1: Graphic representation of the equivalent thermal network solved by Motor-CAD: small circles represent the nodes of the network, rectangles the thermal resistances, and double overlapping circles the thermal power sources and sinks. Network portions relative to the main motor components are grouped and labelled individually for clarity.

and its value depends upon geometric features (L and A) and the material thermal conductivity (λ). The convective resistance is defined through the convective heat transfer coeffcient h_{cnv}

$$R_{\mathrm{cnv}} = \frac{1}{h_{\mathrm{cnv}} A}\,, \tag{2}$$

where h_{cnv} is computed by correlations implemented in the code. Similarly, the radiative resistance is defined as follows

$$R_{\mathrm{rad}} = \frac{1}{h_{\mathrm{rad}} A}\,, \tag{3}$$

and implies linearization of radiative heat transfer. The radiative heat transfer coefficient h_{rad} in Eq. (3) includes surface emissivity and view factors. The contact resistance is modelled as the conductive resistance of a still air gap of the same height as the superficial roughness.

Thermal power sources are constant except for Joule heating in the copper windings. The electric resistivity of copper depends upon temperature, and so does the Joule effect. This is represented as follows

$$P_{\mathrm{wdg}} = P_{\mathrm{ref}} \left[1 + \alpha_{\mathrm{ref}} \left(T - T_{\mathrm{ref}}\right)\right]\,, \tag{4}$$

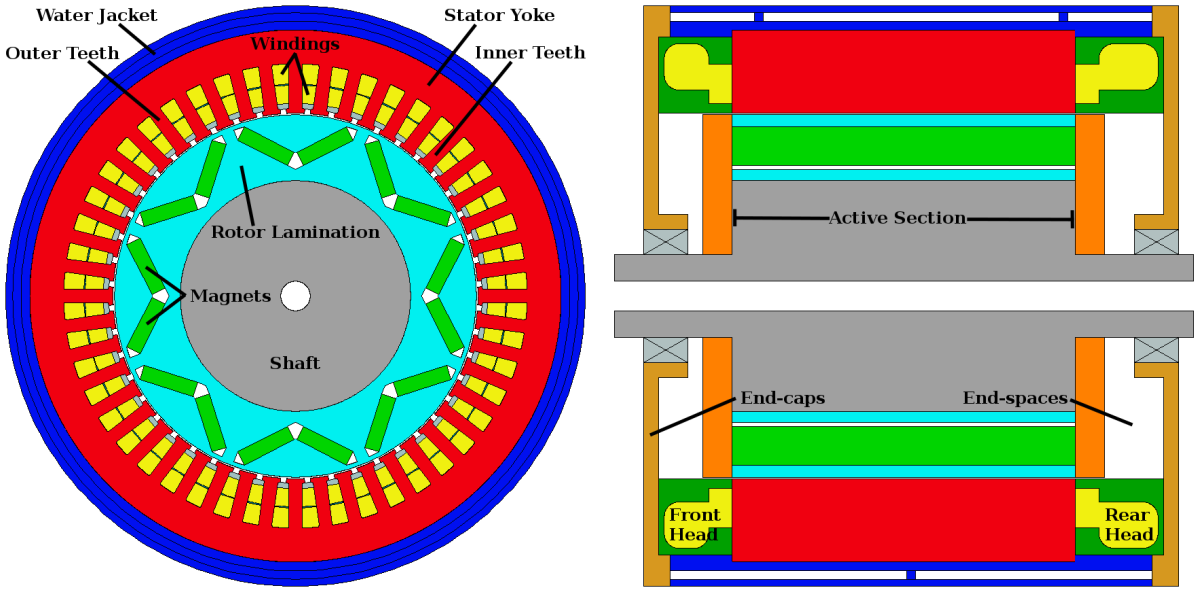

(a) Radial view

(b) Axial view

Figure 2: Radial and axial schematic views of the motor, from Motor-CAD.

where P_{ref} is a fixed value representing the copper losses at T_{ref}, and $\alpha_{\text{ref}} = 3.93 \cdot 10^{-3}\,\text{K}^{-1}$.

Results computed by Motor-CAD include nodal temperatures, heat flows, copper losses, heat transfer coefficients, velocity and pressure drop of the cooling liquid in the water jacket.

3 Motor nominal configuration

The radial and axial views of the motor investigated, corresponding to the thermal network in Fig. 1, are shown in Fig. 2. For clarity, the figure reports also the names of the main components and parts of the motor following the nomenclature used here. The stator has 48 slots for the copper windings, magnets are V-shaped, the stator teeth are parallel, and the shaft is hollow in order to reduce the overall weight and moving masses. According to the FIA Formula E regulation the thickness of the stator lamination must not be smaller than 0.05 mm. Being made of ferromagnetic material, the stator is laminated in order to reduce the eddy current energy losses induced by the variable magnetic flux. The single laminas are then insulated from each other with special coatings.

The LPTN simulations performed are steady-state and correspond to the average load operating condition. The adequacy of the steady approach will be discussed in Section 6 where results of transient analyses over a typical drive cycle are presented.

Thermal sources in an electric motor are to be ascribed to different losses

- electromagnetic losses due to hysteresis and eddy currents in both stator and rotor laminations,
- electromagnetic losses due to Joule effect in the copper windings,
- electromagnetic losses in the insulating materials (usually negligible),

Table 1: Normalized thermal sources in the investigated motor, nominal configuration.

Component	P^*
Copper windings	0.5431
Stator lamination	0.3359
Rotor lamination	0.0969
Magnets	0.0241
Bearings and windage	0.0000
Total	1.0000

Table 2: Normalized temperatures of the main motor parts, nominal configuration.

Part	T^*
Stator yoke	0.425
Stator outer teeth	0.700
Stator inner teeth	0.941
Copper windings	1.000
Rotor magnets	1.663
Rotor lamination	1.670

- mechanical losses due to friction in the bearings and windage in the rotor (usually small and here neglected).

A summary of the normalized thermal sources applied in the present analysis is given in Tab. 1. The normalization for each source follows the formula

$$P^* = \frac{P}{P_{\mathrm{tot,nm}}} \,. \tag{5}$$

The distribution of heat sources in Tab. 1 is derived from electromagnetic simulations based on materials data sheets and experimental data collected at Magneti Marelli, and represents an input for the current study. Resistivity in the windings is measured using calibrated instruments. Detailed FEA where each single wire is modelled are also performed. Losses in stator and rotor are evaluated comparing the thermal fields in bench experiments to FEA.

Conditions summarized above lead to the calculation by Motor-CAD of normalized temperatures of the main motor parts as reported in Tab. 2. The normalization is based on the temperature difference between the windings and the coldest point of the motor which is given by the water at the inlet of the cooling system (water jacket)

$$T^* = \frac{T - T_{\mathrm{wj,in}}}{T_{\mathrm{wdg,nm}} - T_{\mathrm{wj,in}}} \,. \tag{6}$$

The mass-weighted average temperature is considered for the windings, although heads, being immersed in a thick layer of insulating resin, are usually at a higher temperature than the active section.

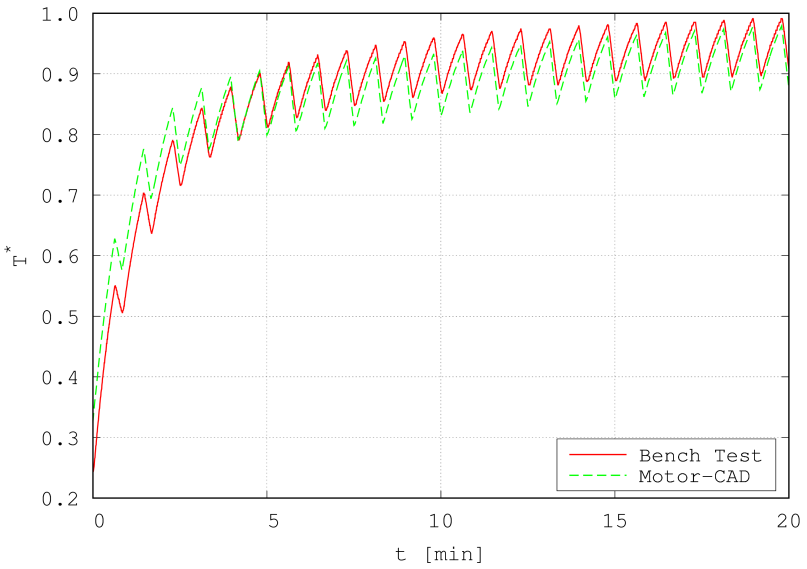

Figure 3: Time history of stator inner teeth temperature: bench experiment *vs* Motor-CAD simulation.

Motor-CAD model is validated against bench experiments performed on the motor for an intermittent load with a 50 s period and average thermal sources as in Tab. 1. Validation results are shown in Fig. 3 where the measured time history of the stator inner teeth temperature compares satisfactorily with the computed one. An almost periodic behaviour is reached in a few minutes, the time-averaged temperature in the last period is 0.945 in the bench experiment, and 0.928 in the transient simulation, the asymptotic temperature being 0.941 according to the steady-state simulation (see Tab. 2).

The hottest part of the motor is the rotor despite its thermal sources amount to only 12 % of the total. This means that the portion of heat discharged externally through the shaft is marginal, and the rotor cooling follows a radial path across the stator. In Fig. 4 the main heat flux paths are shown by subdividing the motor into six macro-components and evaluating the heat transferred in between. Heat fluxes in the figure are normalized as follows

$$\dot{Q}^* = \frac{\dot{Q}}{P_{\text{tot,nm}}} \,. \tag{7}$$

More than 99.5 % of the thermal power generated is dissipated through the water jacket, while the remaining portion is removed by natural convection at the end-caps. Most of the thermal power generated in the windings is transferred to the stator ($\dot{Q} = 0.384$), and it is in part discharged directly to the water jacket through the motor end-windings ($\dot{Q} = 0.125$). Similarly for the rotor where the largest portion of heat flows to the stator through the airgap ($\dot{Q} = 0.069$) while minor portions are subtracted by the shaft and the end-spaces. A substantial heat flux crosses the stator ($\dot{Q} = 0.788$) as it collects the heat generated in the rotor, in the windings, and in the stator itself. Thus, the main heat flux path develops radially from the rotor and the windings, through the stator, to the water jacket. It is of interest to focus on this portion of motor in order to investigate how this heat flux path could be favoured: a reduction of the resistances along the path, in fact, is expected to bring major temperature reductions

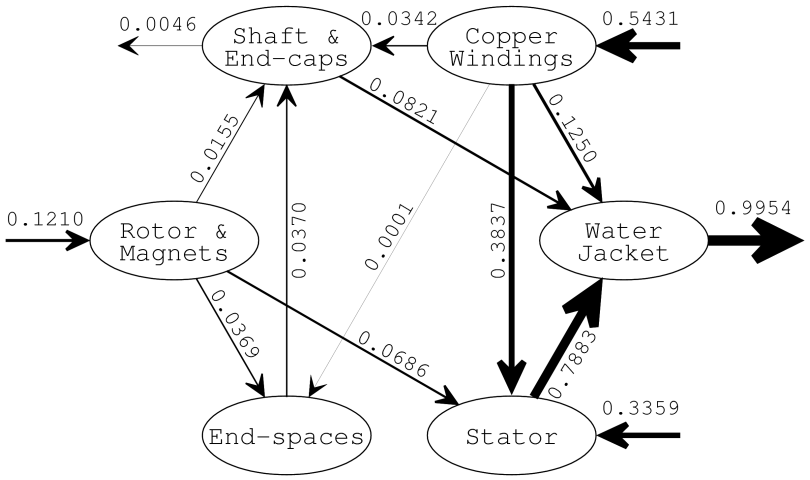

Figure 4: Heat fluxes between different motor components.

in the motor.

The purpose of the present analysis is to suggest possible ways to reduce the motor operating temperatures, with a focus on the average temperature of the copper windings. Since the windings electromagnetic losses depend on temperature, achieving a better cooling also means achieving an improved motor performance in terms of efficiency, power, and torque delivered, which is the true goal of the work. A sensitivity analysis is carried out by first investigating geometrical features and material properties along the main heat flux path. This includes the stator, the windings region, and the water jacket. Afterwards, an optimization study is performed addressing the most important parameters from the sensitivity analysis with the addition of a proper set of constraints.

4 Sensitivity analysis

Sensitivity analysis is done by externally controlling the LPTN model, which includes loading a motor model, modifying the input data and finally running the LPTN simulation. At this stage, the analysis is limited to mono-variate sensitivities, the multi-variate problem will be addressed in Section 5 where an optimization procedure is considered. The parameters included in the sensitivity analysis are listed below:

- rotor and magnets: the analysis is limited to variations in the thermal conductivity of materials,
- airgap: the thickness of the airgap separating the rotor from the stator affects the thermal power exchange from the rotor to the stator,
- windings slots: the structure inside the slot is rather complicated. Each wire is electrically insulated with a thin enamel layer, each bundle of wires is insulated by a coil divider sheet, the wires are immersed in an insulating epoxy resin, and finally the whole content of the slot is insulated from the stator lamination with the slot liner, another sheet of insulating material wrapped around

Table 3: Results of the sensitivity analysis: local sensitivities of the investigated parameters.

Parameter	g^*_{wdg}	Parameter	g^*_{wdg}
stator slot depth	-0.7449	λ slot liner	-0.1239
active length	-0.6076	λ impregnating resin	-0.1088
λ stator lamination	-0.4419	water jacket channel height	$+0.0937$
stator tooth width	-0.3013	λ wire enamel	-0.0636
water jacket mass flow rate	-0.2846	λ coil divider	≈ 0.0
stator yoke thickness	$+0.2503$	λ rotor and magnets	≈ 0.0
water jacket channel width	$+0.2009$	airgap thickness	≈ 0.0

the cavity. As electrically insulating materials are very often also thermally insulating and the thickness of each layer is already very thin in the current motor configuration, the sensitivity analysis is focused on the thermal conductivity of the insulating materials,

- stator: the stator is the motor component crossed by the largest heat flux. The sensitivity analysis is carried out on the thermal conductivity of the stator lamination, and also on some geometrical parameters that affect the slots. These are: tooth width, slot depth, yoke thickness, and active section length,

- water jacket: the water jacket is a rectangular duct shaped as a spiral wrapping the motor. The main parameters influencing the equivalent thermal resistance of the water jacket are water mass flow rate, height, and width of the channel.

Overall the sensitivity analysis addresses 14 parameters: 6 thermal conductivities (rotor and magnets, enamel, coil divider, impregnating resin, slot liner, stator), 7 geometric parameters (airgap thickness, tooth width, slot depth, yoke thickness, active length, water jacket channel height, and width), and 1 operating condition (water mass flow rate in the water jacket). The temperature behavior for some of the most influential parameters is shown in Fig. 5. Data on the abscissas are normalized with respect to the nominal configuration, which is marked by a vertical line in the plots. Every temperature slope tends to become horizontal as its associated resistance is decreased meaning that the thermal bottleneck along the heat flux path is moved somewhere else, and major improvements can only be obtained through multi-variate analysis. In Tab. 3 the local sensitivities for all the investigated parameters are shown in terms of gradients of the normalized average windings temperature with respect to the normalized parameter value at the nominal configuration, that is, for a generic parameter x,

$$g^*_{\mathrm{wdg}} = \left(\frac{\partial T^*_{\mathrm{wdg}}(x^*)}{\partial x^*} \right)_{x^*=1} . \tag{8}$$

As expected, any increment in the thermal conductivity of materials is associated with temperature reductions. Even though the influence of the thermophysical properties of insulating materials might

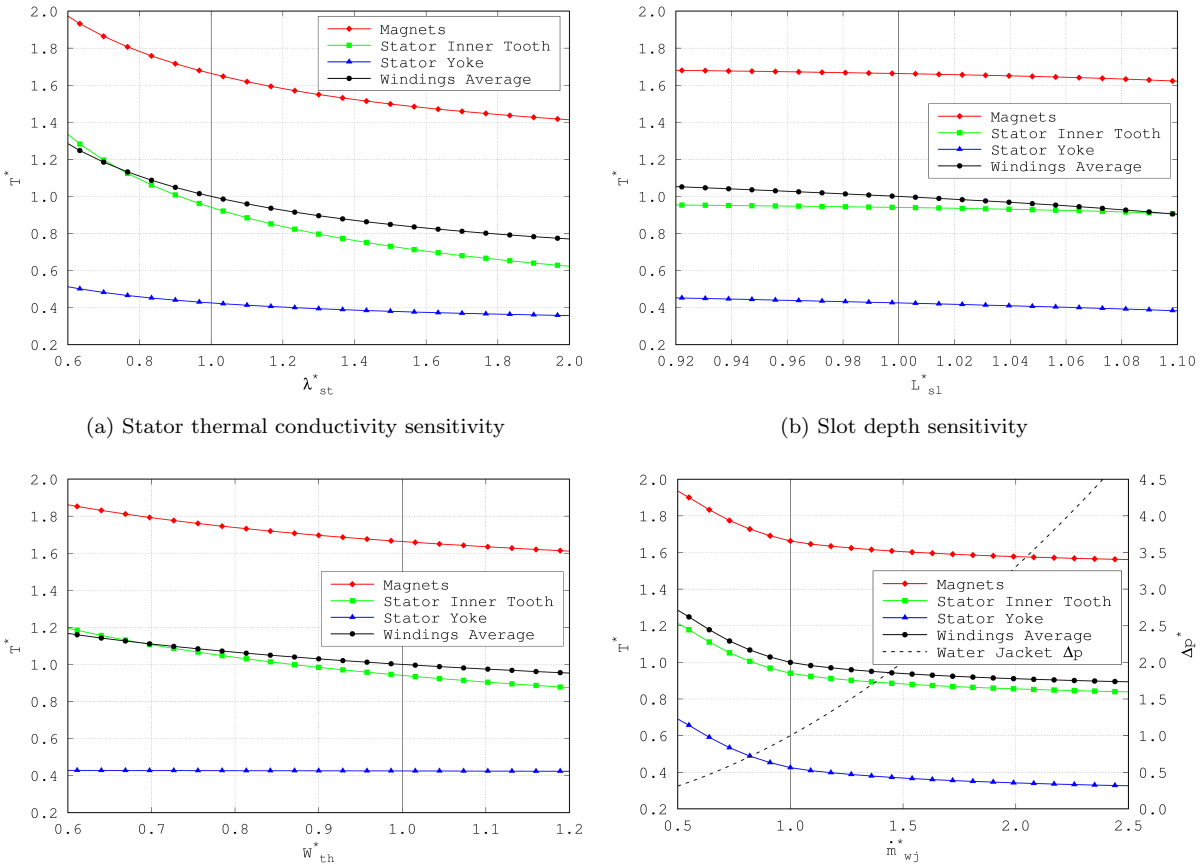

(a) Stator thermal conductivity sensitivity

(b) Slot depth sensitivity

(c) Tooth width sensitivity

(d) Water jacket mass flow rate sensitivity

Figure 5: Results of the sensitivity analysis: normalized temperature trends for some of the investigated parameters. The nominal configuration is marked with vertical lines.

seem relatively small from the inspection of Tab. 3, research has recently brought to significant advances and there may still be room for improvement. For instance, in [18] slot liners of different porosity are tested so that they can be partially impregnated with the more conductive resin. Other studies focus on the resin thermal properties: with the use of suitable additives the thermal conductivity can be increased [19] still preserving other important characteristics. The resin, in fact, must have low viscosity for a high impregnation rate, thermal expansion coefficient as close as possible to the windings and the stator, and high glass transition temperature for avoiding abrupt changes in thermal expansion coefficient while the motor is in operation. As most of the heat fluxes occur through the stator, the thermal conductivity of the stator lamination is also particularly important for limiting the temperature rise of the motor (Fig. 5a).

Concerning the geometry, Tab. 3 shows that several of the geometrical parameters addressed have a considerable impact on the windings thermal behaviour, in particular the stator slot depth (Fig. 5b). Yet, it must be considered that the variation of a single parameter indirectly affects other portions of the motor. For fixed stator inner and outer diameters, larger tooth widths increase the radial heat transfer (Fig. 5c), but this may not leave enough room for the wires in the slots. Smaller yoke thicknesses would

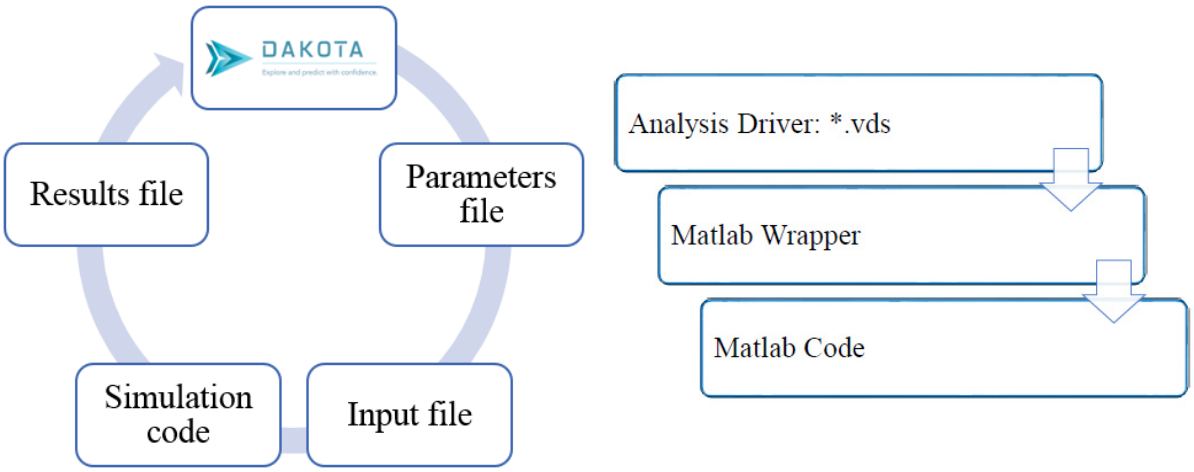

(a) Structure of the optimization process

(b) Structure of the files governing the connection to an external tool (*i.e.* Matlab)

Figure 6: Logical structure for the data processing in Dakota.

again favour the radial heat transfer, but then too much mass would be eroded from the stator so that magnetic saturation of the iron may occur. Longer slot depths lead to larger surface areas through which the thermal power generated in the windings can be transmitted, but also in larger resin fractions in the slots, so that the overall impact may be positive only for thermal conductivities of the resin above a certain threshold. Reducing the hydraulic diameter of the water jacket channel as long as the flow remains turbulent, or incrementing the mass flow rate is always beneficial for the convective heat transfer, but the pressure drop increases quadratically (Fig. 5d). The pressure drop marked by a dashed line in Fig. 5d is normalized with respect to the pressure drop of the nominal configuration

$$\Delta p^*_{\mathrm{wj}} = \frac{\Delta p_{\mathrm{wj}}}{\Delta p_{\mathrm{wj,nm}}} \,. \tag{9}$$

Finally, while Tab. 3 gives an interesting overwiev of the sensitivities in the neighbourhood of the nominal configuration so that the most important parameters can be identified, a mono-variate analysis is not sufficient to define a feasible enhanced motor configuration. A multi-variate optimization involving a proper set of constraints and objective functions must also be performed.

5 Optimization

The optimization of the motor is carried out using the freeware optimization software Dakota. The code has been connected to the LPTN simulation tool through Matlab scripts exploiting the ActiveX commands available in Motor-CAD. Dakota implements many optimization algorithms among which there are local gradient methods, local derivative-free methods, global stochastic methods including the possibility of performing multi-objective optimizations. The logical structure of the data processing in Dakota is sketched in Fig. 6.

Three subsequent optimizations are performed, this approach is motivated by the circumstance that, as explained further in the text, the three steps are found to be essentially independent. The objective of the optimizations is always the minimization of the average temperature of the windings or equivalently, see Eq. (4), the minimization of the windings heat production. In every run the range of variation of the variables is kept relatively large in order to leave broad margins of action to the algorithm. In the nominal configuration the mechanical power needed for granting the coolant mass flow rate is much smaller than 1 W and therefore the pressure drop in the water jacket is small. Considering this, and also that the temperature trend in Fig. 5d sensibly flattens only for normalized mass flow rates around 2, it is decided to fix the mass flow rate at twice the nominal value in all the optimizations. The variables and the constraints addressed vary in each optimization as follows:

1. Optimization of the water jacket: the variables included in the optimization are the height and the width of the water jacket channel. A constraint on the admissible pressure drop across the water jacket is needed for the problem to be well-posed. The constraint is set to 5 times the nominal pressure drop.

2. Optimization of the stator geometry: the variables of the optimization included the slot depth, the tooth width, and the yoke thickness. Due to motor compactness requirements the active length is excluded from the optimization despite its significance. The water jacket channel height and width are set following the results of the first optimization. The constraints applied require that the volume of the slot cavity is large enough to fit the nominal number of wires, and that the stator mass is at least that of the nominal configuration.

3. Optimization of the stator geometry with enhanced thermal conductivities: the previous optimization is repeated after the values of the thermal conductivities of the slot liner and of the impregnating resin are increased.

A detailed resume of the setup of the optimizations is given in Tab. 4 where data are normalized with respect to the nominal configuration values. The Nelder and Mead simplex algorithm [20] is repeated for 5 runs from different starting regions, preceded by a mono-objective genetic algorithm run [21] with a population size of 20 individuals evolving for 50 generations. The results of the optimizations are summarized in Tab. 5 and in Fig. 7, where the same normalization is used.

Let us consider the water jacket first. Once the flow rate, the cross-section, and the length of the channel are known, pressure drop and Nusselt number can be predicted using the canonical formulas for fully developed flow and heat transfer in a duct. From the Nusselt number it is then possible to compute the thermal resistance. Thus, for a given admissible pressure drop, the water jacket channel can be easily optimized by searching for the cross-section shape that allows the highest possible Nusselt number. From Tab. 5 it is noted that by doubling the mass flow rate in the water jacket the losses in the windings are reduced by 1.5 % while the average normalized windings temperature decreases by 9 %. This involves a three times higher pressure drop. The optimization of the water jacket leads to further marginal improvements by reducing the channel height and width up to when the pressure constraint is met. From a preliminary multi-level Full-Factorial Design of Experiments (FF-DOE) it was seen

Table 4: Synoptic table of the optimizations performed.

Optimization Number	Variables and Ranges	Constraints and fixed parameters
1	$0.50 \leq H^*_{\mathrm{wj}} \leq 1.25$	$\dot{m}^*_{\mathrm{wj}} = 2$
	$0.50 \leq W^*_{\mathrm{wj}} \leq 1.25$	$\Delta p^*_{\mathrm{wj}} \leq 5$
2	$1.00 \leq L^*_{\mathrm{sl}} \leq 1.25$	$\dot{m}^*_{\mathrm{wj}} = 2$
	$1.00 \leq W^*_{\mathrm{th}} \leq 1.25$	$L^*_{\mathrm{act}} = 1$
	$0.50 \leq L^*_{\mathrm{yk}} \leq 1.25$	$H^*_{\mathrm{wj}} = 0.911$
		$W^*_{\mathrm{wj}} = 0.957$
		$V^*_{\mathrm{sl}} \geq 1$
		$M^*_{\mathrm{st}} \geq 1$
3	Same as optimization 2	Same as optimization 2, plus
		$\lambda^*_{\mathrm{ln}} = 2$
		$\lambda^*_{\mathrm{rs}} = 2$

that the response surface in terms of average windings temperature has a rather flat optimum region so that actually there are a number of equivalent $(H^*_{\mathrm{wj}}, W^*_{\mathrm{wj}})$ choices for the two variables that as long as they both span in the range [0.8, 1.1] and allow to meet the pressure constraint, they are substantially optimal. For any choice of the variables within the ranges given in Tab. 4 the flow in the water jacket is turbulent with Reynolds numbers in the range between 8×10^3 and 2×10^4. As the convective water jacket thermal resistance does not affect any other resistance of the LPTN, and is thus independent from the other free parameters, there is no need to include the water jacket variables in further optimizations. Parameters resulting from the first optimization stage are thus implemented and kept fixed during the subsequent analyses.

It should be noted in addition that by doubling the mass flow rate and for a fivefold allowable pressure drop, the mechanical power needed to pump the coolant through the water jacket will increase by a factor of ten as

$$P_{wj} = \dot{V}_{wj} \Delta p_{wj} \, . \tag{10}$$

Despite this increase, the mechanical power is still small compared to the gain in terms of reduced losses (see Tab. 5). Instead, a double mass flow rate is expected to have a larger impact on the mechanical power required to pump the coolant through the external pipings and radiator. The performance improvement is apparent in terms of temperature field, but the actual advantage in net motor power output needs to be evaluated in each specific case.

In the second optimization the geometry of the stator is addressed focusing on three parameters: slot depth, tooth width, and yoke thickness. The relevance of the slot depth is already clear from the sensitivity analysis (Tab. 3). However, deeper slots would reduce the mass of the stator lamination leading to possible magnetic saturation of the material. The mass constraint can be recovered with

Table 5: Results of the optimization. The variables of each optimization run are marked in bold, the plus sign identifies the active constraints.

Parameters	Nominal	Modified	Optimization Number		
and Results	Config.	Nominal	1	2	3
H^*_{wj}	1	1	**0.911**	0.911	0.911
W^*_{wj}	1	1	**0.957**	0.957	0.957
L^*_{sl}	1	1	1	**1.201**	**1.201**
W^*_{th}	1	1	1	$\mathbf{1.25}^+$	$\mathbf{1.25}^+$
s^*_{yk}	1	1	1	**0.708**	**0.708**
$\dot{m}^*_{\mathrm{wj}}$	1	2	2	2	2
Δp^*_{wj}	1	3.304	5^+	5	5
V^*_{sl}	1	1	1	1^+	1^+
M^*_{st}	1	1	1	1^+	1^+
λ^*_{ln}	1	1	1	1	2
λ^*_{rs}	1	1	1	1	2
P^*_{wdg} (Eq. (5))	0.5431	0.5347	0.5341	0.5245	0.5145
P^*_{tot} (Eq. (5))	1	0.9916	0.9910	0.9814	0.9714
P^*_{wj} (Eq. (5))	0.0000	0.0002	0.0003	0.0003	0.0003
T^*_{wdg} (Eq. (6))	1	0.9108	0.9049	0.8030	0.6965

thicker teeth, which would also contribute reducing the thermal resistances in the stator, or thicker yokes, which on the contrary would negatively affect the path of heat fluxes. As expected the optimization algorithm tends towards deeper slots, see results in Tab. 5, while the other variables settle compatibly with the constraints of the problem. The first variable reaching the upper range limit is the tooth width. When this happens the algorithm stops increasing the slot depth because the advantage brought by the longer slot is more than counterbalanced by the thicknening of the yoke necessary to satisfy the mass constraint and by the lenghtening of the tooth. The thermally optimized stator geometry allows a further 11 % reduction of the normalized windings temperature obtained with the first optimization step without modifying the stator mass and external diameter.

It should be observed at this point that unlike the changes proposed in optimization #1, the elongated slot shape resulting from optimization #2 can alter significantly the electromagnetic field, with an impact also on the motor efficiency. While it is expected that losses in stator and rotor will be only marginally affected by the changes suggested by optimization #2, longer and thinner slots can result into increased AC losses in the windings, and decreased torque delivered at the given current intensity due to thinner yokes. Torque could be recovered by thickening the yoke at the expense of an increased motor weight and a less efficient heat transfer to the water jacket. The large margins of variations conceded to the variables in this optimization step are expected to emphasize these unwanted electromagnetic effects, thus undermining the constant loss assumption.

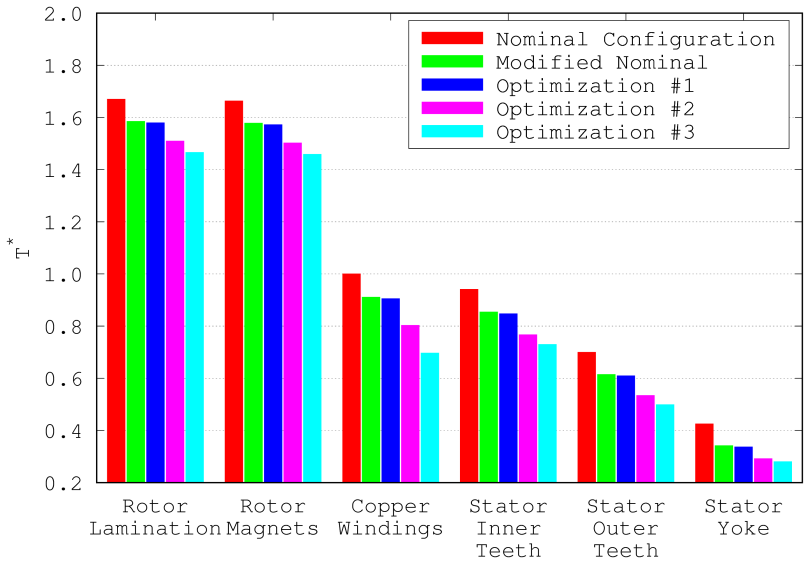

Figure 7: Results of the optimization: temperature trends in the main motor components for the configurations reported in Tab. 5.

As larger conductivities are always beneficial for the thermal management of the motor, results of an optimization of thermal conductivities would be trivial. Instead, the aim of the third optimization is to investigate changes in the optimum stator geometry for insulating materials of enhanced thermal conductivity. The focus is on insulating materials because they are considered the most promising and currently under development. Within the third optimization the stator geometry is addressed again, but after doubling the thermal conductivity of the two most relevant insulating materials (namely, slot liner and resin). The optimum stator geometry does not change due to the predominant significance of the slot depth parameter. With the enhanced thermal conductivities the normalized temperature of the windings drops by another 13 % with respect to the second optimization. Overall, winding losses are thus reduced by more than 5 %.

Figure 7 shows the temperature decrease in the main motor components from the nominal to the various optimized configurations, see the defininition of normalized temperature in Eq. (6) for a correct interpretation. While the first and the second optimizations lead to comparable temperature reductions throughout the motor affecting components that are located downstream to the main heat sources along the heat flux path, the last, having brought changes in the slot area alone, leads to a sensible cooling in the windings region, and to marginal temperature reductions in the rest of the motor.

6 Transient analysis

A transient analysis over a Formula E drive cycle is finally performed on the nominal configuration and after optimization #3. The drive cycle is built starting from real data on a typical street circuit. This provides an estimate of the time required for reaching steady-state operating condition and a measure of amplitude and frequencies of temperature fluctuations. The time history of temperature at selected

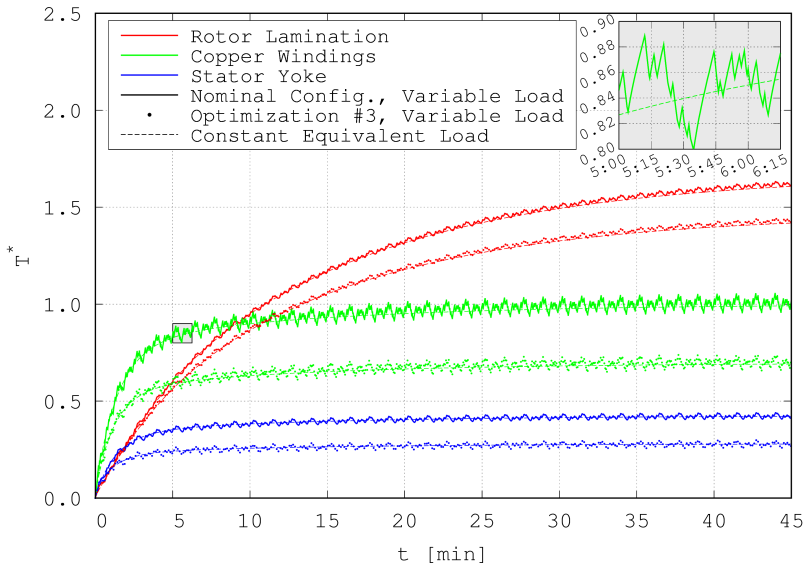

Figure 8: Time history of temperature in windings, rotor lamination, and stator yoke. Continuous thick lines refer to nominal, and dots to optimization #3 configurations. Thin dashed lines show the respective equivalent constant load cases. The top right window shows a zoomed view of the 4^{th} lap for windings.

locations is shown in Fig. 8 for the chosen drive cycle and for its equivalent constant load case, both starting from ambient temperature.

By regulation, Formula E races last approximately 45 minutes, and one lap usually requires around 1 minute and 15 seconds to be completed. Beginning with the 2019 championship, the maximum power output during a race is 200 kW, the motor rotation speed is up to 20 000 rpm, the battery is limited to 54 kWh and should last the whole race. In line with this, Fig. 8 displays results of a transient analysis simulating a 36 laps, 45 minutes full race.

As apparent in Fig. 8 an initial transient and a subsequent statistically steady state can be identified. The transient lasts a few minutes for the stator and windings, while it takes longer for the rotor. Given the small amount of losses and its larger time constant, the rotor is not expected to affect the heat transfer analysis and optimization in the rest of the motor. This is also confirmed by the stator reaching a statistically steady state well before the rotor.

Given that the rate of thermal energy produced by losses in the windings is proportional to the square of the torque while that in the laminations increase with the rotation speed, thermal power production undergoes a steep increase for increasing loads. Therefore, a duty cycle including long periods at high power can deteriorate the motor performance. However, in a street circuit the maximum load is rarely kept for more than a few seconds. This is evident in Fig. 8 where the period of the temperature oscillations induced by accelerations and decelerations is shown to be small. The same holds for the oscillations amplitude that never exceeds $0.1\,T^*$.

Results displayed in Fig. 8 and the discussion above suggest that the thermal analysis and the

optimization performed in steady-state condition are expected to provide results that are relevant to the actual motor.

7 Conclusions

The thermal analysis of a water jacket cooled BPM electric motor developed for the FIA Formula E championship is presented. The investigation is based on LPTN steady-state simulations for given electromagnetic losses under the average load operating condition.

The simulation of the motor in its nominal configuration allows for the identification of the main heat flux path, which extends radially from the stator to the water jacket heat sink. Most of the thermal power generated by electromagnetic losses in the windings, the rotor, and the stator itself is transmitted radially so that the heat flux across the stator sums up to the 79 % of the total losses of the motor.

A sensitivity analysis is performed, focusing on the identification of the main parameters affecting heat management. These include thermal conductivity of materials, geometry of the stator and the water jacket, together with operating condition of the cooling system. The sensitivity analysis has clarified the possible directions for reducing thermal resistances and temperatures.

Finally, a multi-variate optimization performed in three independent steps allows to identify the optimum geometry layout for the water jacket and the stator for given sets of constraints. After step two of the optimization process, the normalized average windings temperature is decreased by 20 % with respect to the nominal configuration; note that at this stage the thermal conductivities are still at their nominal value.

The aim of the analysis presented is the optimal thermal management of prescribed heat losses in the motor. As such, electromagnetic effects brought by geometric changes dictated by thermal considerations are neglected. The inclusion of detailed FEA in the optimization loop would grant a better estimate of the actual losses in each case and could provide directly applicable geometries. Nevertheless, a full optimization procedure would also require a computational effort which is currently non-compatible with applications.

References

[1] F. Endert, T. Heidrich, U. Schwalbe, T. Szalai, and S.D. Ivanov. Effects of current displacement in a PMSM traction drive with single turn coils. In *Proceedings of the 2013 IEEE International Electric Machines & Drives Conference (IEMDC)*, pages 160–165, 2013.

[2] A. Reinap, F.J. Márquez-Fernández, R. Andersson, C. Högmark, M. Alaküla, and A. Göransson. Heat transfer analysis of a traction machine with directly cooled laminated windings. In *Proceedings of the 4th International Electric Drives Production Conference (EDPC 2014)*, pages 1–7, 2014.

[3] C.M. Liao, C.L. Chen, and T. Katcher. Thermal analysis for design of high performance motors. In *Proceedings of the 6th Intersociety Conference on Thermal and Thermomechanical Phenomena in Electronic Systems ITHERM'98*, pages 424–433, 1998.

[4] A. Fasquelle and D. Laloy. Water cold plates cooling in a permanent magnet synchronous motor. *IEEE Transactions on Industry Applications*, 53(5):4406–4413, 2017.

[5] M.-S. Kim, K.-S. Lee, and S. Um. Numerical investigation and optimization of the thermal performance of a brushless DC motor. *International Journal of Heat and Mass Transfer*, 52(5-6):1589–1599, 2009.

[6] D.H. Lim and S.C. Kim. Thermal performance of oil spray cooling system for in-wheel motor in electric vehicles. *Applied Thermal Engineering*, 63(2):577–587, 2014.

[7] K.H. Lee, H.-R. Cha, and Y.-B. Kim. Development of an interior permanent magnet motor through rotor cooling for electric vehicles. *Applied Thermal Engineering*, 95:348–356, 2016.

[8] P.H. Mellor, D. Roberts, and D.R. Turner. Lumped parameter thermal model for electrical machines of TEFC design. *IEE Proceedings B: Electric Power Applications*, 138(5):205–218, 1991.

[9] R. Yabiku, R. Fialho, L. Teran, M.E. Ramos Jr., and N. Kawasaki. Use of thermal network on determining the temperature distribution inside electric motors in steady-state and dynamic conditions. *IEEE Transactions on Industry Applications*, 46(5):1787–1795, 2010.

[10] A. Boglietti and A. Cavagnino. Analysis of the endwinding cooling effects in TEFC induction motors. *IEEE Transactions on Industry Applications*, 43(5):1214–1222, 2007.

[11] A. Boglietti, A. Cavagnino, and A. Staton. Determination of critical parameters in electrical machine thermal models. *IEEE Transactions on Industry Applications*, 44(4):1150–1158, 2008.

[12] D.A. Staton and A. Cavagnino. Convection heat transfer and flow calculations suitable for electric machines thermal models. *IEEE Transactions on Industrial Electronics*, 55(10):3509–3516, 2008.

[13] N. Simpson, R. Wrobel, and P.H. Mellor. Estimation of equivalent thermal parameters of impregnated electrical windings. *IEEE Transactions on Industry Applications*, 49(6):2505–2515, 2013.

[14] X. Liu, H. Yu, Z. Shi, L. Huang, T. Xia, and R. Guo. Porous metal model for calculating slot thermal conductivity coefficient of electric machines. *Applied Thermal Engineering*, 111:981–988, 2017.

[15] J. Bellettre, V. Sartre, F. Biais, and A. Lallemand. Transient state study of electric motor heating and phase change solid-liquid cooling. *Applied Thermal Engineering*, 17(1):17–31, 1997.

[16] O. Wallscheid and J. Böcker. Global identification of a low-order lumped-parameter thermal network for permanent magnet synchronous motors. *IEEE Transactions on Energy Conversion*, 31(1):354–365, 2016.

[17] M. Bernagozzi, S. Charmer, A. Georgoulas, I. Malavasi, N. Michè, and M. Marengo. Lumped parameter network simulation of a loop heat pipe for energy management systems in full electric vehicles. *Applied Thermal Engineering*, 141:617–629, 2018.

[18] R. Wrobel, S.J. Williamson, J.D. Booker, and P.H. Mellor. Characterising the performance of selected electrical machine insulation systems. In *Proceedings of the 2015 IEEE Energy Conversion Congress and Exposition (ECCE)*, pages 4857–4864, 2015.

[19] J. Samek, C. Ondrusek, and J. Kurfurst. A review of thermal conductivity of epoxy composites filled with Al_2O_3 or SiO_2. In *Proceedings of the 19th European Conference on Power Electronics and Applications (EPE'17 ECCE)*, pages P1.–P.6, 2017.

[20] J.A. Nelder and R. Mead. A simplex method for function minimization. *The Computer Journal*, 7(4):308–313, 1965.

[21] D.E. Goldberg. *Genetic algorithms in search, optimization, and machine learning.* Addison-Wesley, 1989.